Naval Research Laboratory
Washington, DC 20375-5320

NRL/7350/MR—2023/4

Testing for Agreement between Human Digitizers and a Machine Learning Algorithm when Digitizing Rip Currents in Time-Averaged Imagery

SARAH TRIMBLE, PH.D

ALLISON PENKO, PH.D

Sediment Dynamics Section
Ocean Sciences Division

August 30, 2023

REPORT DOCUMENTATION PAGE

Form Approved
OMB No. 0704-0188

1. REPORT DATE *(DD-MM-YYYY)*	**2. REPORT TYPE**	**3. DATES COVERED** *(From - To)*
30-08-2023	NRL Memorandum Report	07/2021 – 07/2022

4. TITLE AND SUBTITLE

Testing for Agreement between Human Digitizers and a Machine Learning Algorithm when Digitizing Rip Currents in Time-Averaged Imagery

5a. CONTRACT NUMBER

5b. GRANT NUMBER

5c. PROGRAM ELEMENT NUMBER
NISE

6. AUTHOR(S)

Sarah Trimble and Allison Penko

5d. PROJECT NUMBER

5e. TASK NUMBER

5f. WORK UNIT NUMBER
N200

7. PERFORMING ORGANIZATION NAME(S) AND ADDRESS(ES)

Naval Research Laboratory
4555 Overlook Avenue, SW
Washington, DC 20375-5320

8. PERFORMING ORGANIZATION REPORT NUMBER

NRL/7350/MR--2023/4

9. SPONSORING / MONITORING AGENCY NAME(S) AND ADDRESS(ES)

Naval Research Laboratory
4555 Overlook Avenue, SW
Washington, DC 20375-5320

10. SPONSOR / MONITOR'S ACRONYM(S)

NRL/NISE

11. SPONSOR / MONITOR'S REPORT NUMBER(S)

12. DISTRIBUTION / AVAILABILITY STATEMENT

DISTRIBUTION STATEMENT A: Approved for public release; distribution is unlimited.

13. SUPPLEMENTARY NOTES

Karles Fellowship

14. ABSTRACT

Rip currents result from alongshore variations in wave dissipation; they transport sediment and nutrients within the surfzone but also pose a surf safety hazard. Studying these ephemeral currents is logistically difficult, but remote sensing provides avenues for identifying and tracking rip currents, as well as the bathymetric rip channels which foster rip current development. Machine learning applications can be trained to identify visual signatures in time-averaged optical imagery – where those visual signatures were assumed to signal the presence of a rip channel and/or current. Multiple studies have developed machine learning algorithms to automate the digitization of these visual signatures, which performed well when trained and tested with visual information (only). In this study we investigate the spatial coincidence of rip channels present in lidar bathymetry and the visual signatures they produce in optical time averaged images, as digitized by both a trained machine learner and a group of human digitizers. We found that the majority of target features in the bathymetric data were not signaled by visual signatures, regardless of whether those visual signatures were manually digitized by a group of subject matter experts or automatically by the trained machine learner. These findings suggest that bathymetric depressions may not reliably produce the visual signature in the time averaged imagery, as previously assumed.

15. SUBJECT TERMS

16. SECURITY CLASSIFICATION OF:			**17. LIMITATION OF ABSTRACT**	**18. NUMBER OF PAGES**	**19a. NAME OF RESPONSIBLE PERSON**
a. REPORT	**b. ABSTRACT**	**c. THIS PAGE**			Sarah Trimble
U	U	U	U	25	**19b. TELEPHONE NUMBER** *(include area code)* (228) 688-5671

This page intentionally left blank.

CONTENTS

FIGURES

TABLES

TESTING FOR AGREEMENT BETWEEN HUMAN DIGITIZERS AND A MACHINE LEARNING ALGORITHM WHEN DIGITIZING RIP CURRENTS IN TIME-AVERAGED IMAGERY

1. ABSTRACT

Rip currents result from alongshore variations in wave dissipation; they transport sediment and nutrients within the surfzone but also pose a surf safety hazard. Studying these ephemeral currents is logistically difficult, but remote sensing provides avenues for identifying and tracking rip currents, as well as the bathymetric rip channels which foster rip current development. Machine learning applications can be trained to identify visual signatures in time-averaged optical imagery – where those visual signatures were assumed to signal the presence of a rip channel and/or current. Multiple studies have developed machine learning algorithms to automate the digitization of these visual signatures, which performed well when trained and tested with visual information (only). In this study we investigate the spatial coincidence of rip channels present in lidar bathymetry and the visual signatures they produce in optical time averaged images, as digitized by both a trained machine learner and a group of human digitizers. We found that the majority of target features in the bathymetric data were not signaled by visual signatures, regardless of whether those visual signatures were manually digitized by a group of subject matter experts or automatically by the trained machine learner. These findings suggest that bathymetric depressions may not reliably produce the visual signature in the time averaged imagery, as previously assumed.

2. INTRODUCTION

Rip currents are a naturally occurring nearshore circulation pattern. They form as a result of alongshore variations in wave energy and bathymetry (except purely hydrodynamic rips; Castelle et al., 2016). Rip currents pose a hazard to beachgoers, causing hundreds of fatal drownings worldwide each year (Brewster et al., 2019). They also transport sediment and nutrients within the surf zone. There are several types of rip current, including bathymetric rips, which occur along sandy coasts with three-dimensional morphology (Castelle et al. 2016). The bathymetric rip current type is arguably the most dangerous for beachgoers because it can form under favorable swimming conditions and with variable alongshore location (G. Dusek & Seim, 2013); the bathymetric rip current type is also challenging for beachgoers to visually identify (Brannstrom et al., 2014, 2015) and for scientists to predict (Dalrymple et al., 2011; Radermacher et al., 2018). Bathymetric rip currents are therefore of prime interest for scientific study, yet difficult to observe with in situ field instruments. Remote sensing can provide a relatively low-cost, logistically accessible nearshore observation system for capturing large volumes of bathymetric rip current observations.

Locally installed cameras have been used to observe the development of bathymetric rip currents since the late 1980s. Identification of rip currents in video and images from these cameras was initially performed by human expert digitizers (Ranasinghe et al., 2004) but recent publications have shown that machine learning algorithms can be trained to replicate that digitization process with >98% recall (e.g. de Silva et al., 2021; Maryan et al., 2019). However, the logistical difficulty of observing rip current flow (with in situ instruments or remote sensing) and rip channels (with bathymetric surveys) in conjunction with camera imagery means that relatively few studies have confirmed how often rip currents' appearance in visual imagery correctly signals the presence of an active rip current and/or a bathymetric rip channel. Another possibility is that the visual signature in imagery which has been relied upon since the 1980s indicates either (a) the presence of a rip channel in bathymetry without flow, (b) the presence of offshore directed rip current flow, or (c) both.

Manuscript approved August 25, 2023.

We previously investigated the spatial correspondence between rip currents' appearance in imagery and rip channel presence in bathymetry and found that rip channels' visual signature in imagery was much less reliable than previously assumed (Trimble et al. 2022); however, that study relied upon a trained machine learner for identification of rip channels in imagery. The poor spatial correspondence observed between bathymetric rip channels and visual signatures in imagery may not repeat with a group of human digitizers. This study investigates spatial correspondence between rip channel presence in bathymetry, rip channels identified by a machine learner, and rip channels identified by human digitizers. Results can inform whether visual signatures consistently indicate rip channels, regardless of digitizer (human or machine learner).

2.1 Remote sensing of bathymetric rip currents

Since the development of Argus and similar camera systems in the 1980s (Lippmann & Holman, 1989, 1990), multiple studies have utilized video imagery to observe wave height (Aarninkhof & Ruessink, 2004; Almar et al., 2012; Andriolo, 2019), celerity (Holland et al., 1991), run-up (R. A. Holman & Guza, 1984; Simarro et al., 2015), surface currents (Chickadel, 2003), and the location of maximized or minimized wave breaking. Averaging 10 minutes of video frames at 1 – 2 Hz creates a time-averaged image that highlights variations in wave breaking (Holman & Stanley, 2007) where areas of consistent wave breaking are dominated by white surface foam recorded as higher-intensity pixels in the RGB time-averaged image (greater than 200 on an 8-bit scale of 0–255; example shown in Figs. 1 and 4). Local maxima in pixel values spatially correspond with local maxima in bathymetric elevations under specific environmental conditions, revealing the location of the sandbar (Holman et al., 2013; Simarro et al., 2019; Thuan et al., 2019). Therefore, time-averaged imagery can be used to track changes in the location of a sandbar crest through time (Guedes et al., 2011; Mallet et al., 2000; Pape et al., 2010; Ruessink et al., 2009).

Evidence shows a similar spatial correspondence exists between the local minima in pixel intensity and local minima in wave breaking (Bruneau et al., 2009; R. A. Holman et al., 2006; MacMahan et al., 2005) where the decreased wave breaking may be caused by: (a) lower bathymetric elevations, (b) the offshore-directed flow of a rip current, or (c) both. The interaction of alongshore variations in coastal morphology and incident wave angles creates variations in wave height and wave breaking alongshore, where areas of increased wave breaking (high-intensity pixels) generate increased set-up on the beach, which are adjacent to areas of less wave breaking and less set-up (lower intensity pixels). In addition, the adjacent regions of high and low set-up can generate a pressure gradient that causes the focused, offshore-directed flow of a rip current (Castelle et al., 2016; Haller, 2002). Both a rip channel and/or a rip current may cause the decreased wave breaking that appears in time-averaged imagery but to date, no study has quantified whether either cause is consistent. Panels C and D in Fig. 1 show how a region of relatively low-intensity pixels can appear as a narrow, shore-normal feature intersecting the regions of high-intensity pixels that result from breaking waves. Throughout the remainder of this paper, the term "visual signature" is used to refer to this shore-normal region of low-intensity pixels intersecting the high-intensity pixels of the surf zone in time-averaged imagery.

2.2 Visual signatures in time averaged imagery

Figure 1 is a timeline of the pioneering efforts in utilizing pixel intensity in time-averaged images to estimate the locations of local maxima and minima in nearshore bathymetry. Initial research qualitatively demonstrated a spatial correspondence between local maxima in cross-shore transects of time-averaged image pixel intensity and field-surveyed bathymetry (Lippmann & Holman, 1989, 1990; Figure 1a). Increased accessibility and accuracy of survey technology by the early 2000s enabled comparisons between

spatially dense bathymetric surveys and time-averaged imagery to reveal that higher elevations and higher-intensity pixels could be spatially correspondent throughout an image, not only in the cross-shore direction (Konicki & Holman, 2000; Ruessink et al., 2000; van Enckevort & Ruessink, 2001; Figure 1b).

Holman et al. (2003) were the first to suggest that spatial correspondence between local maxima in wave breaking and pixel intensity implied a matching spatial correspondence between local minima in wave breaking and pixel intensity, suggesting that the lowered wave breaking apparent in time-averaged images indicated the location of lowered bathymetry (i.e. bathymetric rip channels) and/or the offshore directed flow of a bathymetric rip current. In the years that followed, visual signatures in time-averaged imagery were utilized to track the alongshore location of flowing rip currents (Holman et al., 2006) and rip channels (Gallop et al., 2011; Orzech et al., 2010; Quartel, 2009; Splinter et al., 2011) often citing Holman et al. (2003) and Ranasinghe et al. (2004). Yet, while Holman et al. (2003) include a comprehensive review of supporting observations prior to that publication date, it does not contain quantitative analysis of pixel intensity and bathymetric observations or observations of rip current flow. Ranasinghe et al. (2004) are often cited as the pioneering evidence that a reliable spatial correspondence exists between visual signatures and rip channels. However, they validated rip channel presence with a threshold of 70% agreement between human digitizers of time-averaged images and did not include an analysis of bathymetric observations.

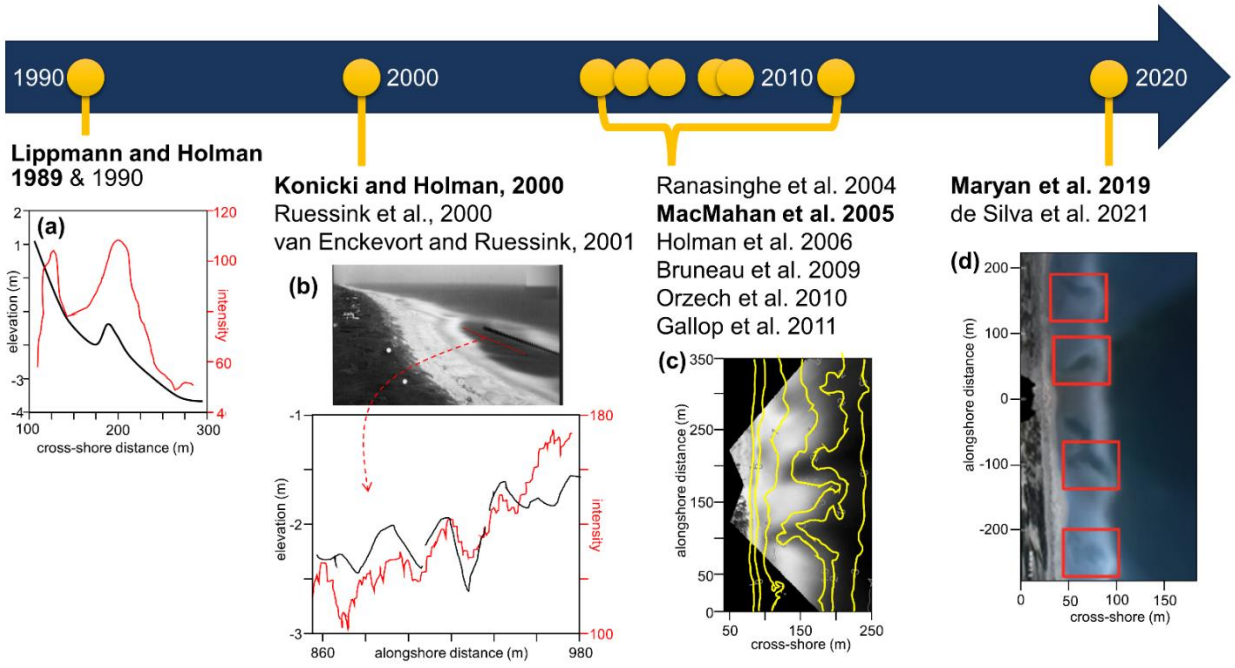

Fig. 1—Examples of research developments using time-averaged imagery to track areas of wave breaking (and lack thereof). Bold citations indicate the source of the adapted plot shown below. (a) The first papers to use video cameras for remotely observing the near shore showed that maximums of pixel intensity (red line) and elevation (black line) had spatial correspondence in 2D cross-shore transects. (b) Following studies showed spatial correspondence may exist in alongshore transects between local minimums of pixel intensity and local minimums of elevation; note that the intensity profile (red) is not from the exact location as the elevation profile (black). (c) Qualitative spatial correspondence was observed between visual signatures (background grayscale) and shore-normal channels observed in bathymetry (yellow contour lines). (d) Machine learning methods can automate the detection and digitization of visual signatures (red boxes) in time-averaged images (background image) with a 98% accuracy rate.

2.3 The use of machine learning for identification of visual signatures

Multiple field campaigns since 2004 have collected time-averaged imagery and bathymetric observations showing spatial correspondence can exist between visual signatures and rip channels (Bruneau et al., 2009; MacMahan et al., 2005; Moulton, Elgar, et al., 2017) as well as rip flow (MacMahan et al., 2005; Moulton et al., 2017a; Fig. 1c) but to date only Trimble et al. (2022) has quantified how often the visual signature indicates the presence of a rip channel. Trimble et al. (2022) found that spatial correspondence between visual signatures and rip channels was inconsistent, with <4% of visual signatures correctly indicating the presence of a narrow, shore normal depression in the bathymetry indicative of a rip channel. They were not able to evaluate the spatial correspondence between visual signatures and rip current flow. They also relied on a trained machine learner for visual signature identification; a different machine learner or a group of human digitizers may have generated different results.

Despite a lack of quantitative evidence that visual signatures reliably indicate either a rip current or a rip channel, recent papers have used machine learning and deep learning methods to automate the identification of visual signatures in time-averaged imagery (A. de Silva et al., 2021; Maryan et al., 2019; Rashid et al., 2021). In these efforts, machine learning algorithms were trained and tested with a set of images annotated by a group of experts. The trained machine learners achieved ≥98% accuracy in identifying visual signatures in imagery (de Silva et al., 2021; Maryan et al., 2019) and video (de Silva et al., 2021, 2023). However, these studies make no assertions as to the reliability of an identified visual signature accurately indicating the location of either a rip channel or a flowing rip current.

2.4 Motivation

The present body of literature has established that high-intensity pixels in cross-shore transects of time-averaged imagery are spatially correspondent with areas of increased wave breaking and higher elevations (Lippmann and Holman, 1990, 1989). In addition, a similar spatial correspondence can exist between low-intensity pixels in alongshore transects and with rip channels or rip currents (Konicki and Holman, 2000; Ruessink et al., 2000; van Enckevort and Ruessink, 2001), but the reliability of that spatial correspondence is not yet quantified. The decreased wave breaking that generates the visual signature may be the result of either (1) lowered elevations within a rip channel, (2) an actively flowing rip current, or (3) both. No study has yet quantified how often (or the conditions under which) the visual signature represents each of these causes. In addition, Trimble et al. (2022) demonstrated that the machine-learner identified visual signatures indicated <3% of rip channels and <7% of all bathymetric depressions in the data. Despite the uncertainties surrounding the reliability of a visual signature indicating the presence of a rip channel and/or rip current, multiple studies have produced machine learning algorithms that can replicate the digitization of visual signatures historically produced by human digitizers in time-averaged images (Maryan et al., 2019) and satellite images and video (de Silva et al., 2021, 2023). To responsibly progress this line of research, it is necessary to quantify the frequency with which a visual signature indicates a rip channel. Future research can investigate how often the visual signature indicates the location of a flowing rip current. **We investigate how often visual signatures identified by human digitizers spatially correspond to rip channels in bathymetry. We also investigate whether those results are replicated by a trained machine learner. Results can inform whether visual signatures consistently indicate rip channels, regardless of digitizer (human or machine learner).**

3. APPROACH

Our primary aim was to determine whether the presence of a rip channel in the surf zone would be consistently indicated by visual signatures, where those visual signatures were digitized by humans or a machine learner. The following subsection 2.1 describes the study site and field data collection. Subsection 2.2 describes the digitization of rip channels, and subsection 2.3 describes the digitization of visual signatures. Subsection 2.4 describes the methods employed to calculate the spatial and temporal correspondence between digitized visual signatures and bathymetry. Subsection 2.5 describes our analysis of the influence of wind and wave conditions on the results. A final subsection 2.6 summarizes the overall workflow.

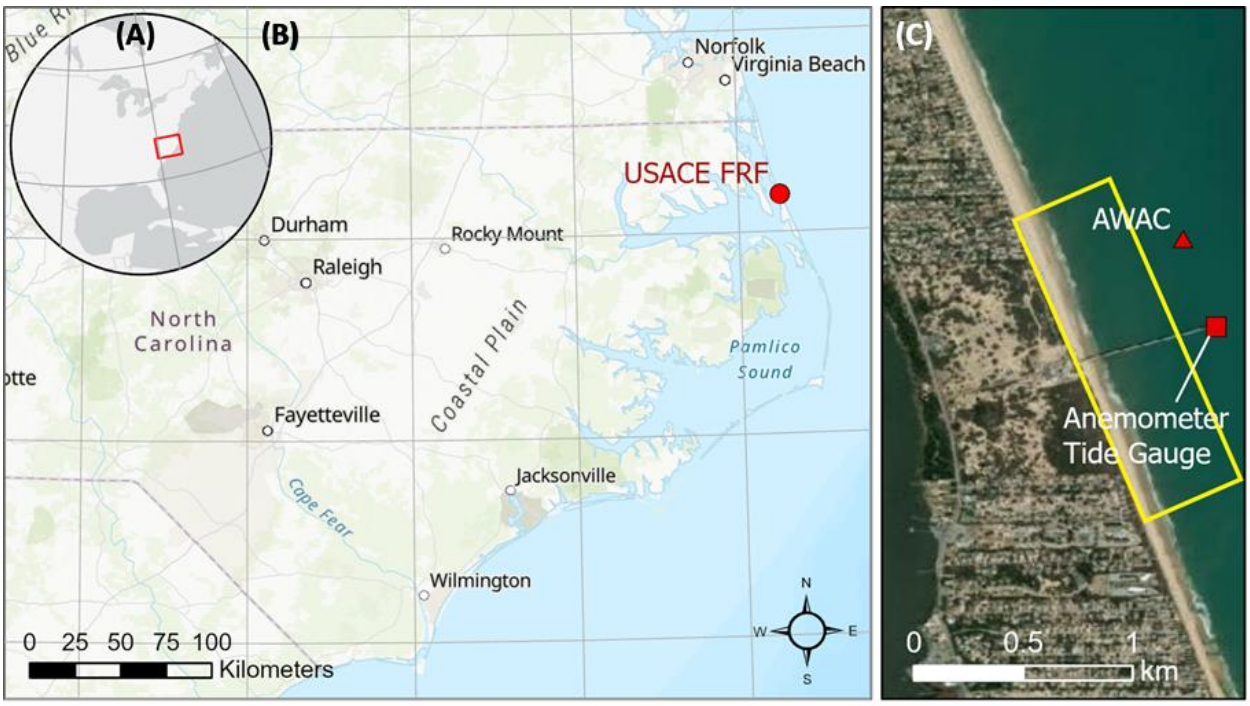

Fig. 2—The location of the USACE FRF in Duck, North Carolina, USA. (A) Circle inset map at the upper left shows the eastern United States, with a red box indicating the extent of (B) the map of coastal North Carolina. The FRF is located on the northern Outer Banks barrier island chain of North Carolina. Panel (C) shows satellite imagery of the FRF, the footprint of time-averaged images used (yellow outline) and locations of field instruments (red symbols). Data used for this figure are courtesy of Esri, USGS, GeoEye, and the State of North Carolina Department of Transportation.

3.1 Field Observations

All imagery and field measurements of bathymetry, wind, and waves were collected at the United States Army Corps of Engineers' (USACE) Field Research Facility (FRF) Coastal Hydraulics Lab (CHL) located in Duck, North Carolina, USA (Fig. 2). Tides at the site are semidiurnal with a mean range of ~1m (Birkemeier et al., 1985). Water levels were sampled every 6 minutes by a NOAA tide station (ID#8651370) located at the end of the FRF pier. Wave data were sampled hourly by a bottom-mounted, upward-looking Nortek AWAC at 6 m depth. Wind observations were sampled by an R.M. Young marine anemometer

mounted at the end of the FRF pier, 19.36 m above sea level. Reported wind speeds and directions were vector averaged at 1 Hz over the 10-min sampling period. The locations of these instruments are shown in Fig. 2c.

Surf zone imagery was obtained from an array of cameras mounted on a tower recording RGB images at 2 Hz. Each time-averaged image was created by averaging 1,200 frames collected by the cameras over 10 minutes at the top of every daylight hour. Images were retrieved from the archives of the Coastal Imaging Lab (CIL) at Oregon State University (OSU) and were georectified into real-world coordinates. Only images collected within ±12 hours of the lidar bathymetric observations were used. Images cover a 1.5-km stretch of beach at the site. Over- or underexposed images were removed from analysis and portions of images affected by camera malfunctions were masked from the analysis. The resulting dataset consisted of 51 viable images over four days.

Bathymetric observations are from four lidar data sets provided by the National Oceanic and Atmospheric Association (NOAA) Office for Coastal Management (OCM). Per the industry standard: lidar surveys were processed into digital elevation models (DEMs) by averaging observations into an output cell size 4 to 5 times the average point spacing of observations. The resulting DEMs have horizontal resolutions of 5 m (2013-09-26 and 2015-10-31), 1.35 m (2016-07-02), and 3 m (2019-06-19). Global Positioning System (GPS) times recorded in the raw lidar files show each survey was collected within a 4-hour window. It is reasonable to assume that the bathymetry observed did not undergo significant changes during that time. The morphologies captured by lidar represent various stages of the intermediate beach morphologies described by Wright and Short (1984) and are representative of the study site. The relatively straight beach often has one sandbar within depths of 1 – 2 m and a second bar within depths of 4 – 5 m (Plant et al., 1999; U.S. ACE FRF, 2012).

3.2 Digitizing Rip Channels

Rip channel width is variable because channel cross-section shape can vary widely. Rip channel length is typically 1 – 2 times the width of the surf zone, and channel depth is the vertical distance from mean water level to the thalweg. In general, rip channels have a relief $\geq$ 1 m from surrounding morphology (Brander & Cowell, 2003). Velocities are faster in narrower channels with constrained cross-sectional area, and/or greater relief (Brander, 1999).

We systematically identified locations of rip channels in the lidar-derived DEMs using a Geographic Information System (GIS) to follow the methods of Brander and Cowell (2003). For each of the four lidar data sets, a fifth-order polynomial trend was calculated for all elevations between the shoreline (0 m) and a 150 m Euclidean distance in the offshore direction. Subtracting a DEM from its trend surface identifies all regions in the nearshore bathymetry comprised elevations below that trend. These below-trend regions are hereafter called “bathymetric depressions.” Bathymetric depressions were additionally labeled as a rip channel when sufficiently narrow (the ratio of its maximum offshore extent to its maximum alongshore extent was >1.0) and shore-normal (longest axis across was perpendicular to shore ±45°). Rip channels are therefore a subset of the regions labeled as bathymetric depressions. Figure 3 shows a vertically exaggerated 3D rendering of a DEM with outlines of bathymetric depressions and rip channels.

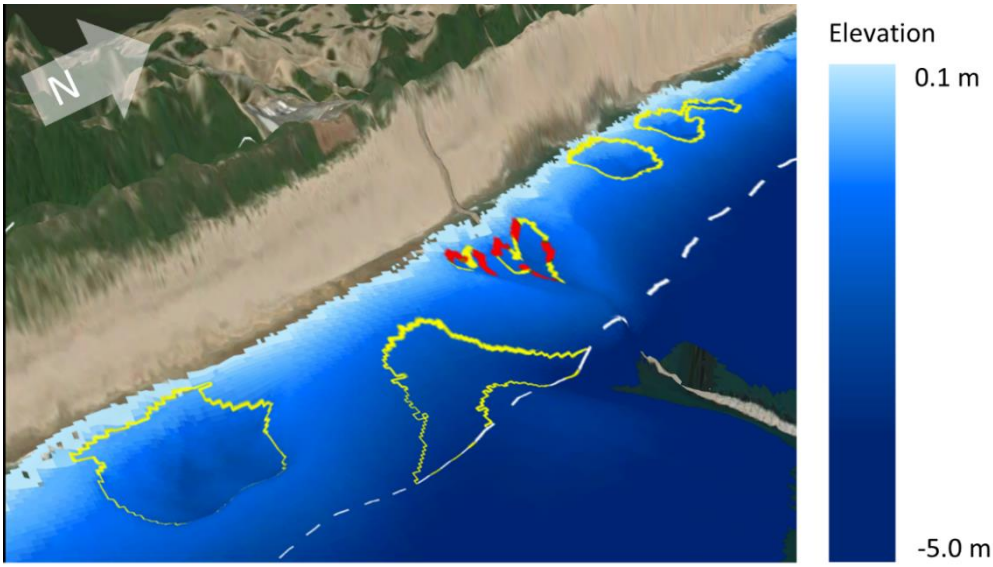

Fig. 3—A 3-D extruded graphic of part of the DEM for 2019-06-19. Satellite imagery has been draped over elevations above the 0-m contour. The increasingly saturated blue pixels are DEM elevations in the near shore (see color bar at right). Bathymetric depressions identified by de-trending are outlined in yellow. Two bathymetric depressions at the center (marked with a red-and-yellow dash) also meet the definition of a rip channels. The dashed, white line shows the seaward boundary of the area analyzed, a 150-m buffer from the shoreline.

3.3 Digitizing Visual Signatures

This study evaluates how often visual signatures identified by human digitizers spatially correspond to rip channels in bathymetry, and how those results compare to a trained machine learner. A visual signature is a shore-normal region of low-intensity pixels intersecting the high-intensity pixels of the surf zone in time-averaged imagery. Previous research utilizing visual signatures in time-averaged imagery relied upon a group of 5 or more humans to outline visual signatures in an image set, then used a threshold agreement to finalize visual signature location (e.g., 70% agreement among digitizers; see Ruessink et al., 2000 and Ranasinghe et al., 2004 for examples). We followed this method, utilizing 7 digitizers and requiring 71% agreement or ≥5/7 digitizers. Digitizers looked at each georectified image in a GIS and outlined any visual signatures they saw. Digitizing was performed without collaboration. A GIS was used to combine these polygons and retain only spaces digitized by ≥5/7 digitizers (Fig. 4).

We also utilized the trained machine learner (ML) published by Maryan et al. (2019) which has a 98% recall for visual signatures in time-averaged imagery. The ML is an object classifier, specifically a Viola-Jones cascade with a meta-classifier backend (Ada-Boost). It was trained with 102 images of Secret Harbour, WA, Australia and our study site, Duck, NC, USA; that image set contained 514 examples of visual signatures. After training with 70% of that data, the ML was able to recall 98% of the visual signatures in the test data. Input to the trained object classifier is a single band (blue) of the time-averaged image, where pixel values are the intensity (0–255). It utilizes a cascade of Haar features to determine if a segmented version of the pixel space is a sufficient match for a narrow, shore-normal pattern indicative of visual signatures. The output is the RGB version of the input image with the addition of red boxes around each identified visual signature (examples shown in Fig. 1d). For more details on the object classifier, its training, and evaluation, see Maryan et al. (2019).

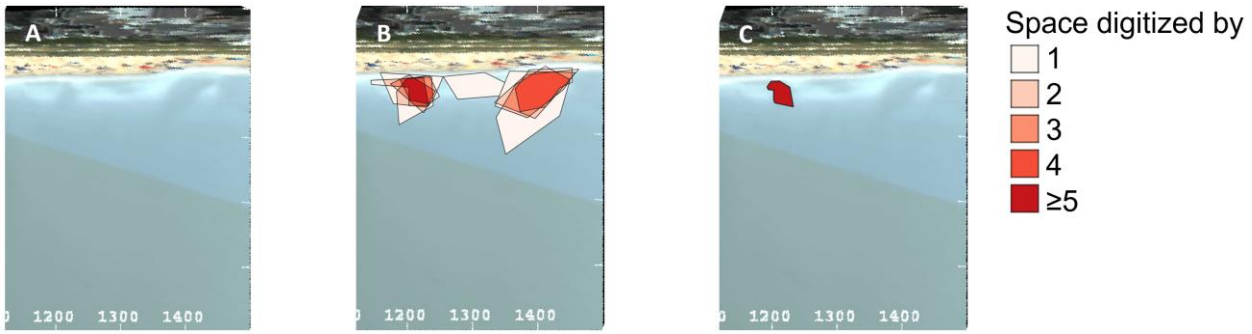

Fig. 4—A portion of the time averaged image from 2019-06-19 1100 EDT. The beach is across the top and numbers along the bottom reflect a local coordinate system (in m) used to georectify the images. (A) Two possible visual signatures are located near the 1200 m and 1400 m alongshore positions. (B) The digitizers' polygons are colored to indicate overlap between digitizers. Key is on the far right. (C) Only spaces with >71% agreement are retained in the human digitized visual signature dataset. Note: the machine learner did not identify any visual signatures in this area of this image

3.4 Calculating Spatial Correspondence

Spatial correspondence between digitized visual signatures and bathymetry was tabulated with a GIS, by both count of occurrence and by area. Spatial correspondence occurred when a digitized visual signature and bathymetric feature had ≥19.6% overlap. The 19.6% threshold represents the proportion of a rectangular visual signature digitization produced by the ML that would overlap with an idealized ellipsoidal rip channel, if 50.1% of that ellipsoid was within the rectangular digitization of the visual signature and the longest axes of both objects were the same size. Table 1 defines true positive, false positive, and false negative outcomes. Outcomes were used to calculate recall and precision, where:

$$Recall = \frac{True\ Positives}{True\ Positives + False\ Negatives}$$

$$Precision = \frac{True\ Positives}{True\ Positives + False\ Positives}$$

Recall describes the percentage of bathymetric features indicated by digitized visual signatures. Precision describes the percentage of digitized visual signatures that indicated a bathymetric feature. For both ratios, values closer to 1.0 indicate better spatial correspondence. Spatial correspondence was calculated between rip channels and human digitized visual signatures, as well as machine learner digitized visual signatures. In addition, to evaluate whether our definition of a rip channel was too restrictive, we calculated spatial correspondence between digitized visual signatures and all bathymetric depressions, which are those depressions identified by the de-trending described in Section 2.2 but without restrictions on size, shape, or orientation. We used a GIS to calculate both (a) how often features in these categories qualified as true positive, false positive, or false negative outcomes and (b) the cumulative area in square meters of each outcome (Table 1). In summary, we investigated eight different definitions of spatial correspondence between digitized visual signatures and bathymetric features (Table 2).

Table 1—All Possible Outcomes of Spatial Correspondence Analysis

Outcome	Definition	By Count	By Area
True Positive	≥ 19.6% of the visual signature overlaps with a bathymetric feature	Add 1 to cumulative sum of true positive cases	Add the area of the object ID to the cumulative sum of true positive area
False Positive	< 19.6% of the visual signature overlaps with a bathymetric feature	Add 1 to cumulative sum of false positive cases	Add the area of the object ID to the cumulative sum of false positive area
False Negative	< 50% of a bathymetric feature overlaps with the area of one or more visual signatures	Add 1 to cumulative sum of false negative cases	Add the area of the bathymetric feature to the cumulative sum of false negative area

Table 2—All Spatial Correspondence Scenarios Analyzed

		Method	
Digitized by	**Target bathymetric feature**	**By Count**	**By Area**
Human digitizers	All bathymetric depressions	Recall & Precision	Recall & Precision
	Rip channels	Recall & Precision	Recall & Precision
Machine Learner	All bathymetric depressions	Recall & Precision	Recall & Precision
	Rip channels	Recall & Precision	Recall & Precision

3.5 Summarizing the Effect of Oceanographic Conditions on Spatial Correspondence

Oceanographic conditions were summarized with ten independent variables: wavelength, wave height, wave period, wave steepness, incident wave direction (relative to shore-normal), water level, the cross-shore component of wind velocity, the direction of the maximum wind vector (relative to shore-normal), the Iribarren number and the Ursell number. We also determined which images were captured during the conditions revealed by the NOAA rip current forecast model to be associated with an increased likelihood of rip presence and intensity (Dusek 2011; Dusek & Seim, 2013).

The Iribarren number (Ir), also called the surf similarity parameter, quantifies the transition from non-breaking to breaking waves (Iribarren and Nogales, 1949),

$$Ir = \frac{\tan\beta}{\sqrt{H/L}},$$

where H is wave height, L is wavelength, and β is the beach slope. The Ursell number (U) quantifies the relationship between wave conditions and water depth and is given by

$$U = \frac{H \cdot L^2}{h^3},$$

where h is the depth of the water column (Ursell, 1953). These dimensionless values are commonly used to characterize the relationship between waves and bathymetry, which is described by beach slope in the Iribarren number and by depth in the Ursell number.

When calculating the correlation between these variables and recall or precision, Pearson correlation (i.e. linear regression) is a common statistic but Pearson assumes data are normally distributed. We performed a one-sample Kolmogorov-Smirnov test to evaluate the null hypothesis (at the 5% significance level) that the observations came from a standard normal distribution and found that we could not reject the null hypothesis for any of the observed variables. This is not unexpected, given that the relationships between wave height, wind speed, and other data analyzed are often nonlinear. Therefore, for our non-normally distributed data, we calculated Spearman's rank correlation, which does not have the normal distribution assumption and is used to reveal relationships that are monotonic even if they are not linear.

3.6 Workflow

This section summarizes sections 2.1 – 2.5. Lidar surveys of the study site were processed into digital elevation models (DEMs). Those DEMs were detrended, following Brander and Cowell (2003), to reveal all bathymetric depressions. The revealed depressions were labeled as rip channels if they were sufficiently narrow and shore-normal. All viable images from within 24 hours of each lidar survey were acquired from the archives hosted by the OSU CIL and georectified into real-world coordinates using a GIS. A group of 7 human digitizers independently reviewed each image and digitized any visual signatures observed. A GIS was used to identify all spaces digitized by ≥5 humans. Spatial correspondence was calculated between the digitized visual signatures and bathymetry. The three outcomes described in Table 1 were calculated with two methods (by count and by area) to determine recall and precision for the eight definitions of spatial correspondence described in Table 2. Field observations were used to generate ten variables describing the oceanographic and geomorphological conditions during each time-averaged image. Correlation statistics were calculated to describe the influence of those ten variables on recall and precision for the eight definitions of spatial correspondence. Findings were compared to a similar study evaluating spatial correspondence between bathymetry and visual signatures digitized by a trained machine learner. Results are discussed in the following Section 3.

4. RESULTS

Visual signatures were identified in 51 images captured on 4 dates. All images were captured within ±12 hours of lidar bathymetry. We evaluated whether human digitized visual signatures were spatially correspondent with bathymetry, and compared those results with the spatial correspondence of visual signatures digitized by a trained machine learner. We also evaluated the effect of wind, waves, and water levels on results. Because previous qualitative research has shown that visual signatures can correspond with rip channels, we anticipated that some spatial correspondence would exist between visual signatures and all bathymetric depressions, but that a higher correspondence would be observed with rip channels. However, these were not the results we observed.

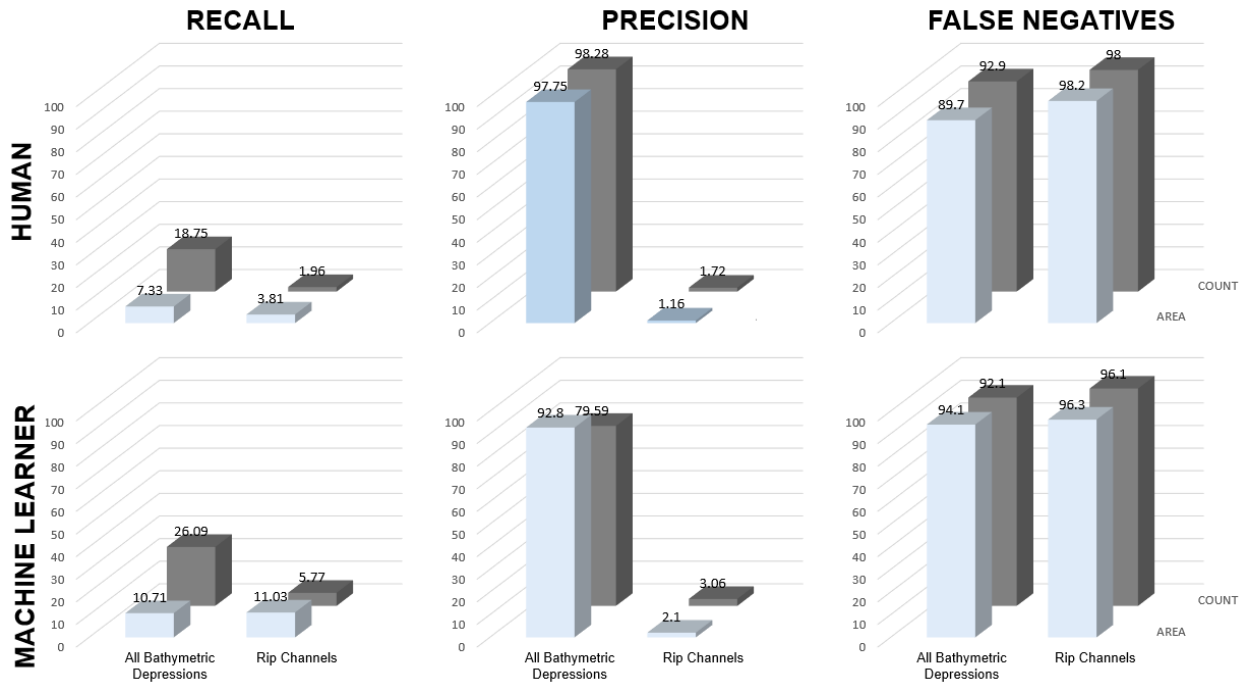

Fig. 5—Recall (left), precision (center), and percentage of all targets that were false negatives (right), when visual signatures are digitized by a group of humans (top panels) or a machine learner (bottom panels) and the target (bottom axes) is either rip channels or all bathymetric depressions, with results tallied either by count or by area (right axes).

4.1 Spatial Correspondence between visual signatures and bathymetry

We summarized spatial correspondence with recall and precision (Fig. 5). Recall is the percentage of target features that are indicated by a digitized visual signature. When digitized by humans, visual signatures recall few rip channels (1.96% by count, 3.81% by area) and recall slightly more of all bathymetric depressions (18.75% by count, 7.33% by area). Precision reveals the percentage of correct indications. When digitized by humans, visual signatures' precision for rip channels was low (1.72% by count, 1.16% by area) but precision was high for all bathymetric depressions (98.28% by count, 97.75% by area). However, visual signatures digitized by humans only indicated a small percentage of all bathymetric depressions (7.1% by count; 10.3% by area) or rip channels (2.0% by count; 1.8% by area) present in the lidar bathymetry, with the majority of both targets remaining false negatives unindicated by human digitized visual signatures.

We compared these results to the recall and precision for the same bathymetry and image set when visual signatures were digitized by a trained machine learner (Trimble et al. 2022) where the same trends were observed (Fig. 5). When digitized by a trained machine learner, visual signatures recalled few rip channels (5.77% by count or 11.03% by area) and recalled slightly more of all bathymetric depressions (26.09% by count or 10.71% by area). When digitized by a trained machine learner, visual signatures precision for rip channels was low (3.06% by count, 2.10% by area) but precision was high for all bathymetric depressions (79.59% by count or 92.80% by area). However, visual signatures digitized by a machine learner only indicated a small percentage of all bathymetric depressions (7.9% by count; 5.9% by area) or rip channels (3.9% by count; 3.7% by area) present in the lidar bathymetry, with the majority of both targets remaining false negatives unindicated by machine learner digitized visual signatures. For nearly

all of these results, statistics were slightly better when visual signatures were digitized by the trained machine learner (Fig. 5).

4.2 The Effect of Oceanographic Conditions on Results

Spearman correlations were calculated to evaluate relationships between 10 oceanographic parameters and spatial correspondence, as measured by precision and recall. For all correlations, relationships were considered significant when $R2 \geq 0.60$ and $p \leq 0.05$. We also investigated how often conditions likely to produce rip currents occurred during image capture.

4.2.1 Differences in Correlated relationships for different target features

When rip channels were the target and visual signatures were digitized by humans, neither precision nor recall was significantly correlated to any of the oceanographic variables analyzed (Fig. 6 A & B, red bars would have been present if any relationships had $p \leq 0.05$). However, when rip channels were the target and visual signatures were digitized by the trained machine learner (Fig. 6 A & B, blue bars), precision and recall were both significantly and negatively correlated with increased wave height (by count & by area R2 = -0.60 for both). Other relationships with $p \leq 0.05$ were not significant ($R2 < 0.60$).

When all bathymetric depressions were the target and visual signatures were digitized by humans, neither precision nor recall was significantly correlated with any of the oceanographic variables analyzed (Fig. 6 C & D, red bars). However, when all bathymetric depressions were the target and visual signatures were digitized by the trained machine learner, precision was significantly correlated with six oceanographic variables (Fig. 6C, blue bars). This precision was negatively correlated with increased wave period (by count and by area both R2 = -0.60), wave direction relative to shore (by count and by area both R2 = -0.79), and wavelength (by count: R2 = -0.67; by area: R2 = -0.68). This precision was positively correlated with wave height (by count: R2 = 0.82; by area: R2 = 0.83), wave steepness (by count: R2 = 0.83; by area: R2 = 0.85), and Iribarren number (by count: R2 = 0.83; by area: R2 = 0.85). Recall of all bathymetric depressions, when visual signatures were digitized by a trained machine learner, was significantly correlated only with wavelength (by area: R2 = -0.64; Fig. 6D, blue bars). It is noteworthy that increasing wave height had negative correlations with recall and precision when rip currents were the target, yet these correlations were positive when all bathymetric depressions were the target.

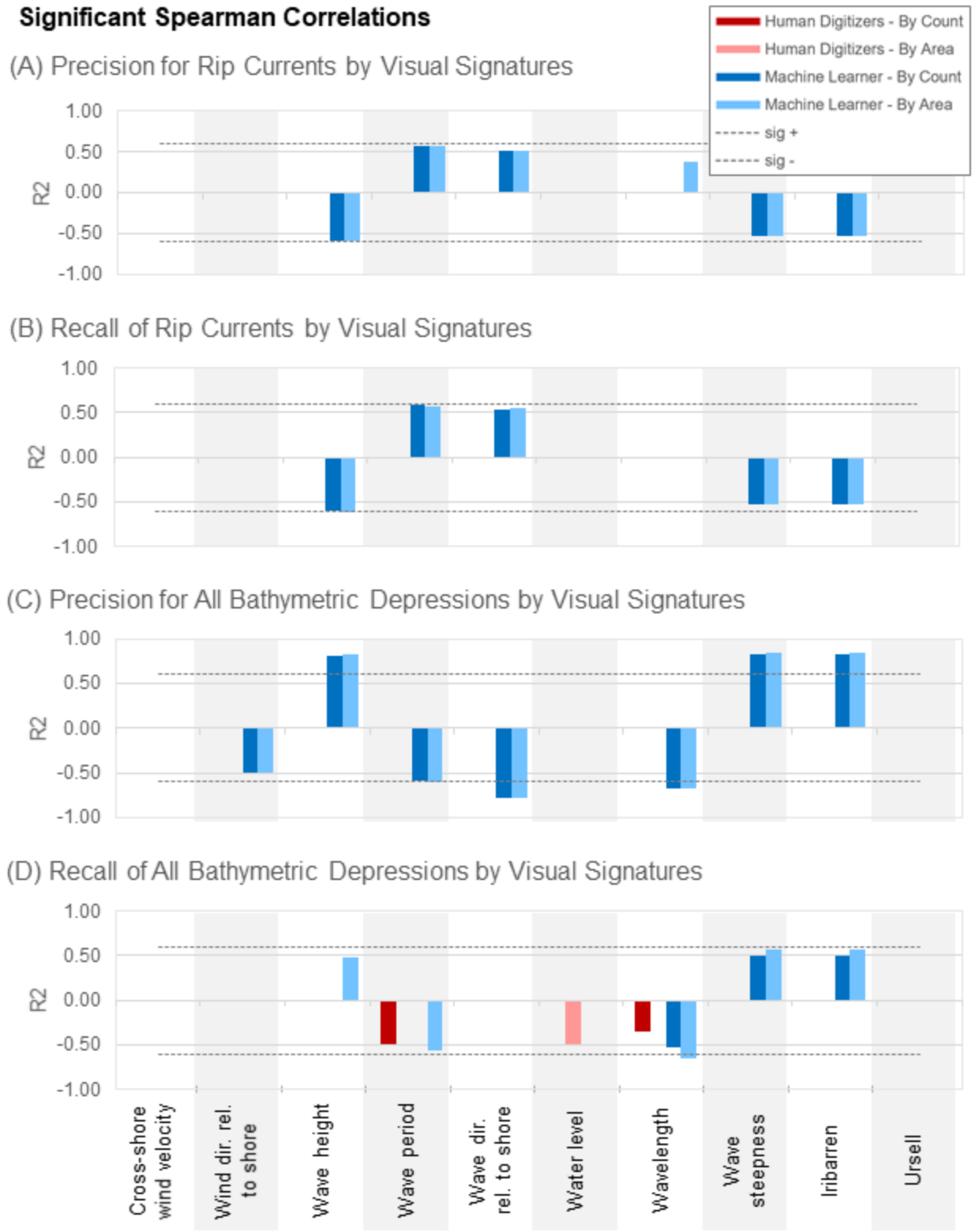

Fig. 6—Significant correlations between oceanographic conditions and results. Only values with $p \leq 0.05$ are shown; a blank space indicates a relationship with $p > 0.05$. Dashed lines at R2 = 0.60 and -0.60 highlight which relationships exceeded these thresholds of significance.

4.2.2 The effect of rip-probable conditions on recall and precision

We did not collect sufficient observations to identify whether a flowing rip current was present at specific locations within the study area during the time-averaged images. However, we can investigate whether conditions were likely to generate rip currents within the region at the time of each image using observed waves, water levels, and winds. Significant wave height is the primary driver of rip current formation. Rip currents in this area are probable when waves are ≥0.7 m, with rip currents persisting up to 1 day after significant wave events (Dusek and Seim 2013). During the dates we studied, Hs was ≥0.7 m in the late afternoon of 2013-09-26, throughout 2015-10-31, and briefly in the 24 hrs before images studied from 2016-07-02 (Fig. 8). Mean wave direction plays a secondary role in rip current development. Rip currents are more likely and more intense when the incident wave angle is closer to shore normal (Dusek and Seim 2013). During the dates studied, waves were closest to shore normal on 2013-09-26 and 2015-10-31 (Fig 8). Low and outgoing tides are associated with increased rip current presence (Dusek et al., 2011; Brander, 1999; Brander and Short, 2000; Bruneau et al., 2009; MacMahan et al., 2005) and each date of this study included a full tidal cycle (Fig. 8). In summary: of the four dates studied, conditions were most likely to produce rip currents on 2015-10-31 (Hs > 0.7 m and relatively shore-normal waves) and any rip currents present on that date would have been strongest during the falling and low tide (images at 0700, 0800, and 0900). We performed a two-sided t-test between those rip-probable images and the images collected during other conditions (where df=48 & α=0.05 ∴ t=2.048; see Table 3). Arrows in Table 3 indicate whether the average statistic was higher or lower for images captured during rip-probable conditions. Rip-probable conditions increased recall and precision for all bathymetric depressions but decreased recall and precision for rip channels (regardless of digitizer, humans or the machine learner).

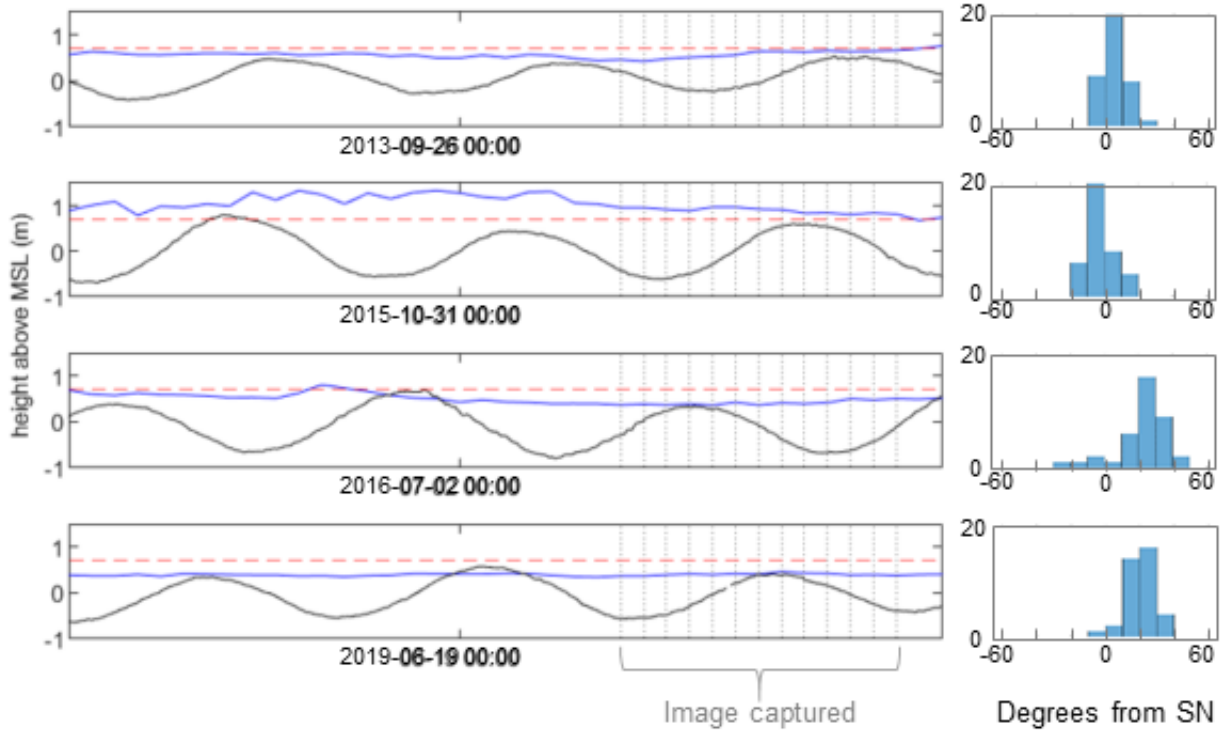

Fig. 7—Oceanographic conditions during each date studied. Data displayed are from 24 hours prior to the first time averaged image until 2 hours after the final image capture. Times series plots (left) show water level (black) and H_s (blue) with a dashed red line at 0.7 m, which is the threshold wave height for rip current generation at the site. Vertical gray lines indicate when a valid time averaged image was captured. Histograms on the right show wave spectra frequency from 1 hour before to 1 hour after the images, in degrees from shore normal.

Table 3—Results of a two-sided t-test between images collected during and outside rip probable conditions. Recall and precision were significantly different for images captured during v. outside rip-probable conditions, where df=48 & α=0.05 ∴ t=2.048, and values >t indicate statistically different populations. The only statistic not significantly impacted by rip-probable conditions was precision (gray t values, lower right) when all bathymetric depressions were the target and visual signatures were digitized by the machine learner. Arrows indicate whether the average statistic was higher (up, green) or lower (down, red) for images captured during rip-probable conditions.

Target	Method	Human Digitizers	Machine Learner
Recall			
Rip channels	By count	4.169 ↓	2.683 ↓
	By area	4.169 ↓	2.749 ↓
All bathymetric depressions	By count	21.904 ↑	13.009 ↑
	By area	14.351 ↑	8.917 ↑
Precision			
Rip channels	By count	5.479 ↓	8.595 ↓
	By area	5.479 ↓	8.179 ↓
All bathymetric depressions	By count	5.479 ↑	0.605
	By area	5.234 ↑	1.286

5. DISCUSSION

Qualitative evidence supports the use of visual signatures to indicate rip channels (Holman et al., 2003; Orzech et al., 2010; Quartel, 2009; Ranasinghe et al., 2004; Splinter et al., 2011). However, to date, only Trimble et al. (2022) specifically investigated the spatial correspondence between rip channels and visual signatures in time-averaged images without a priori knowledge that a rip channel would occur within the study area. They found that visual signatures identified by the same machine learner used in this study only indicated 4% of the rip channels present in the data. We evaluated whether those results were replicated by a group of human digitizers; the method we used here, threshold agreement amongst a group of human digitizers, has been the historic method for identifying rip channels in time-averaged images (e.g. Ranasinghe et al. 2004; Holman et al. 2006; Turner et al. 2007; Orzech, et al. 2010; Loureiro et al. 2012).

5.1 Are visual Signatures Consistently Spatially Correspondent to Rip Channels?

Recall for all methods of analysis was poor (<27%, Fig. 5, left). Precision, or the likelihood that a digitized visual signature correctly indicated a target, was poor for rip channels (<3.1%) but high when the target was expanded to all bathymetric depressions (>79.6%) for both human digitizers and the machine learner (Fig. 5, center). Therefore, visual signatures are precise indicators of all bathymetric depressions identified by the de-trending methods used here (Brander and Cowell 2003) as the vast majority of digitized visual signatures indicate a depression, whether digitized by humans or a trained machine learner (and regardless of tabulation method, by count or by area; Fig. 5, center). However, all possible methods of analysis resulted in a vast majority of targets as false negative (>89.7%), as both targets were poorly indicated by any method of digitizing or analysis (right plots in Fig 5, right). Therefore, a hypothetical study of these dates which relied on visual signatures to indicate either rip channels or all bathymetric depressions would have missed the vast majority of both targets.

5.2 How Is Spatial Correspondence Affected by Oceanographic Conditions?

Previous analysis revealed some correlative relationships between spatial correspondence (when visual signatures were digitized by a trained machine learner) and oceanographic conditions, as measured by 10 quantitative independent variables (see Table 4 and Trimble et al. 2022). In this study, spatial correspondence between bathymetry and visual signatures digitized by a group of humans was poor under all oceanographic conditions and therefore not correlated to changes in the environment. It is possible that the conditions during the four days examined did not allow a wide enough range of oceanographic conditions to properly evaluate relationships between the environment and results; additional research (of a larger range of locations, dates, and conditions) may reveal different relationships between human digitized visual signatures and oceanographic variables. In this study, precision and recall values for visual signatures digitized by humans were relatively similar to values when visual signatures were digitized by the machine learner.

Table 4—All significant correlations ($R2 \geq 0.60$ & $p \leq 0.05$) for visual signatures digitized by the machine learner; no such relationships were found for visual signatures digitized by humans.

	By Count		By Area	
	R2	p	R2	p
Target: Rip Channels				
Precision				
Wave height	-0.60	0.01	-0.60	0.01
Recall				
Wave height	-0.60	0.01	-0.61	0.01
Target: All bathymetric depressions				
Precision				
Wave height	0.82	0.00	0.83	0.00
Wave period			-0.60	0.01
Wave direction relative to shore	-0.79	0.00	-0.79	0.00
Wave length	-0.67	0.00	-0.68	0.00
Wave steepness	0.83	0.00	0.85	0.00
Iribarren number	0.83	0.00	0.85	0.00
Recall				
Wave length			-0.64	0.01

4.2.1 Summary of Trimble et al. 2022 – when visual signatures were digitized by a machine learner

When rip channels were the target, increased wave height was associated with lower precision and lower recall for visual signatures digitized by a machine learner, meaning that increased wave heights increased both false negative and false positive indications of rip channels (Table 3). When the target was all bathymetric depressions, recall was negatively associated with wavelength, where longer wavelengths decreased the likelihood that a bathymetric depression would be indicated by a visual signature. Precision was associated with six oceanographic variables. A visual signature was more likely to be a true positive for all bathymetric depressions when: wave heights increased, wave steepness increased, and the Iribarren number increased. However, a visual signature was more likely to be a false positive when: the wave period increased, the incident wave angle was farther from shore normal, and wavelengths were longer (Table 3).

4.2.2 Visual signatures under rip-probable conditions

A total of 7 images were captured during rip-probable conditions: H_s > 0.7 m, relatively shore-normal waves, and a falling tide. Rip-probable conditions during an image had a significant impact on recall and precision, regardless of whether the target was rip channels or all bathymetric depressions, regardless of whether statistics were tallied by count or by area, and regardless of whether humans or the machine learner digitized the visual signatures – except for precision for all bathymetric depressions when visual signatures were digitized by the machine learner (Table 3). Rip-probable conditions increased recall and precision for all bathymetric depressions but decreased recall and precision for rip channels (regardless of digitizer, humans or the machine learner). One possible interpretation of these statistics is that the offshore directed flow of a rip current was present through many features within the 'all bathymetric depressions' group under rip probable conditions, generating the strong contrast in wave breaking that defines the visual signature and increasing the likelihood that both the human digitizers and the machine learner would identify visual signatures. Unfortunately, no observations of flow can be used to verify or reject that hypothesis.

6. CONCLUSIONS

We investigated how well visual signatures identified by human digitizers were spatially correspondent with rip channels in bathymetry, and found that the majority of rip channels were not indicated by visual signatures. We found the same results when the target was expanded to all bathymetric depressions. These results mirrored the findings of Trimble et al. (2022) which found that visual signatures digitized by a trained machine learner were not spatially correspondent to either rip channels or all bathymetric depressions present in lidar bathymetry. We found some correlations between oceanographic conditions and results, where increased wave height, increased wave period, increasingly shore parallel waves, longer wavelengths, steeper waves, and larger Iribarren numbers could have an effect on recall and precision – although correlations were only found for some methods of analysis. We performed a two-sided t-test to evaluate whether recall and precision for 7 images captured during rip-probable conditions varied significantly from recall and precision for images captured outside rip-probable conditions, and we found that rip-probable conditions increased recall and precision for all bathymetric depressions but decreased recall and precision for rip channels (regardless of digitizer, humans or the machine learner). Future research may investigate whether results repeat for additional dates and locations.

(All Reference Titles are Unclassified)

7. REFERENCES

Aarninkhof, S. G. J., & Ruessink, B. G. (2004). Video observations and model predictions of depth-induced wave dissipation. *IEEE Transactions on Geoscience and Remote Sensing*, *42*(11), 2612–2622. https://doi.org/10.1109/TGRS.2004.835349

Almar, R., Cienfuegos, R., Catalán, P. A., Michallet, H., Castelle, B., Bonneton, P., & Marieu, V. (2012). A new breaking wave height direct estimator from video imagery. *Coastal Engineering*, *61*, 42–48. https://doi.org/10.1016/j.coastaleng.2011.12.004

Andriolo, U. (2019). Nearshore Wave Transformation Domains from Video Imagery. *Journal of Marine Science and Engineering*, *7*(6), 186. https://doi.org/10.3390/jmse7060186

Birkemeier, W. A., Miller, H. C., Wilhelm, S. D., DeWall, A. E., & Gorbics, C. S. (1985). *A user's guide to the coastal engineering research center's (CERC's) field research facility*. Department of the Army US Army Corps of Engineers.

Brander, R. W. (1999). Field observations on the morphodynamic evolution of a low-energy rip current system. *Marine Geology*, *157*(3–4), 199–217. https://doi.org/10.1016/S0025-3227(98)00152-2

Brander, R. W., & Cowell, P. J. (2003). A trend-surface technique for discrimination of surf-zone morphology: Rip current channels. *Earth Surface Processes and Landforms*, *28*(8), 905–918. https://doi.org/10.1002/esp.489

Brannstrom, C., Lee Brown, H., Houser, C., Trimble, S., & Santos, A. (2015). "You can't see them from sitting here": Evaluating beach user understanding of a rip current warning sign. *Applied Geography*, *56*, 61–70. https://doi.org/10.1016/j.apgeog.2014.10.011

Brannstrom, C., Trimble, S., Santos, A., Brown, H. L., & Houser, C. (2014). Perception of the rip current hazard on Galveston Island and North Padre Island, Texas, USA. *Natural Hazards*, *72*(2), 1123–1138. https://doi.org/10.1007/s11069-014-1061-3

Brewster, B. C., Gould, R. E., & Brander, R. W. (2019). Estimations of rip current rescues and drowning in the United States. *Natural Hazards and Earth System Sciences*, *19*(2), 389–397. https://doi.org/10.5194/nhess-19-389-2019

Bruneau, N., Castelle, B., Bonneton, P., Pedreros, R., Almar, R., Bonneton, N., Bretel, P., Parisot, J.-P., & Sénéchal, N. (2009). Field observations of an evolving rip current on a meso-macrotidal well-developed inner bar and rip morphology. *Continental Shelf Research*, *29*(14), 1650–1662. https://doi.org/10.1016/j.csr.2009.05.005

Castelle, B., Scott, T., Brander, R. W., & McCarroll, R. J. (2016). Rip current types, circulation and hazard. *Earth-Science Reviews*, *163*, 1–21. https://doi.org/10.1016/j.earscirev.2016.09.008

Chickadel, C. C. (2003). An optical technique for the measurement of longshore currents. *Journal of Geophysical Research*, *108*(C11), 3364. https://doi.org/10.1029/2003JC001774

Dalrymple, R. A., MacMahan, J. H., Reniers, A. J. H. M., & Nelko, V. (2011). Rip currents. *Annual Review of Fluid Mechanics*, *43*, 551–581.

de Silva, A., Mori, I., Dusek, G., Davis, J., & Pang, A. (2021). Automated rip current detection with region based convolutional neural networks. *Coastal Engineering*, *166*, 103859. https://doi.org/10.1016/j.coastaleng.2021.103859

Dusek, G. (2011). *Daily to yearly variations in rip current activity over kilometer scales*. Doctoral dissertation, University of North Carolina, Chapel Hill, NC.

Dusek, G., & Seim, H. (2013). Rip Current Intensity Estimates from Lifeguard Observations. *Journal of Coastal Research*, *288*, 505–518. https://doi.org/10.2112/JCOASTRES-D-12-00117.1

Gallop, S. L., Bryan, K. R., Coco, G., & Stephens, S. A. (2011). Storm-driven changes in rip channel patterns on an embayed beach. *Geomorphology*, *127*(3–4), 179–188. https://doi.org/10.1016/j.geomorph.2010.12.014

Guedes, R. M. C., Calliari, L. J., Holland, K. T., Plant, N. G., Pereira, P. S., & Alves, F. N. A. (2011). Short-term sandbar variability based on video imagery: Comparison between Time–Average and Time–Variance techniques. *Marine Geology*, *289*(1–4), 122–134. https://doi.org/10.1016/j.margeo.2011.09.015

Haller, M. C. (2002). Experimental study of nearshore dynamics on a barred beach with rip channels. *Journal of Geophysical Research*, *107*(C6), 3061. https://doi.org/10.1029/2001JC000955

Holland, K. T., Holman, R. A., & Sallenger, A. H. (1991). Estimation of overwash bore velocities using video techniques. In *Coastal Sediments* (pp. 489–497). ASCE.

Holman, R. A., & Guza, R. T. (1984). Measuring run-up on a natural beach. *Coastal Engineering*, *8*(2), 129–140. https://doi.org/10.1016/0378-3839(84)90008-5

Holman, R. A., & Stanley, J. (2007). The history and technical capabilities of Argus. *Coastal Engineering*, *54*(6–7), 477–491. https://doi.org/10.1016/j.coastaleng.2007.01.003

Holman, R. A., Symonds, G., Thornton, E. B., & Ranasinghe, R. (2006). Rip spacing and persistence on an embayed beach. *Journal of Geophysical Research*, *111*(C1), C01006. https://doi.org/10.1029/2005JC002965

Holman, R., Plant, N., & Holland, T. (2013). cBathy: A robust algorithm for estimating nearshore bathymetry: The cBathy Algorithm. *Journal of Geophysical Research: Oceans*, *118*(5), 2595–2609. https://doi.org/10.1002/jgrc.20199

Iribarren, R. and Nogales, C., 1949. Protection des ports. XVII International Navigation Congress, Lisbon, Section II-4

Konicki, K. M., & Holman, R. A. (2000). The statistics and kinematics of transverse sand bars on an open coast. *Marine Geology*, *169*(1–2), 69–101. https://doi.org/10.1016/S0025-3227(00)00057-8

Lippmann, T. C., & Holman, R. A. (1989). Quantification of sand bar morphology: A video technique based on wave dissipation. *Journal of Geophysical Research*, *94*(C1), 995. https://doi.org/10.1029/JC094iC01p00995

Lippmann, T. C., & Holman, R. A. (1990). The spatial and temporal variability of sand bar morphology. *Journal of Geophysical Research*, *95*(C7), 11575. https://doi.org/10.1029/JC095iC07p11575

MacMahan, J. H., Thornton, E. B., Stanton, T. P., & Reniers, A. J. H. M. (2005). RIPEX: Observations of a rip current system. *Marine Geology*, *218*(1–4), 113–134. https://doi.org/10.1016/j.margeo.2005.03.019

Mallet, C., Kingston, K. S., Davidson, M. A., & Huntley, D. A. (n.d.). *The use of video in the study of sandbar dynamics*. 6.

Maryan, C., Hoque, M. T., Michael, C., Ioup, E., & Abdelguerfi, M. (2019). Machine learning applications in detecting rip channels from images. *Applied Soft Computing*, *78*, 84–93. https://doi.org/10.1016/j.asoc.2019.02.017

Moulton, M., Dusek, G., Elgar, S., & Raubenheimer, B. (2017). Comparison of Rip Current Hazard Likelihood Forecasts with Observed Rip Current Speeds. *Weather and Forecasting*, *32*(4), 1659–1666. https://doi.org/10.1175/WAF-D-17-0076.1

Moulton, M., Elgar, S., Raubenheimer, B., Warner, J. C., & Kumar, N. (2017). Rip currents and alongshore flows in single channels dredged in the surf zone. *Journal of Geophysical Research: Oceans*, *122*(5), 3799–3816. https://doi.org/10.1002/2016JC012222

Orzech, M. D., Thornton, E. B., MacMahan, J. H., O'Reilly, W. C., & Stanton, T. P. (2010). Alongshore rip channel migration and sediment transport. *Marine Geology*, *271*(3–4), 278–291. https://doi.org/10.1016/j.margeo.2010.02.022

Pape, L., Plant, N. G., & Ruessink, B. G. (2010). On cross-shore migration and equilibrium states of nearshore sandbars. *Journal of Geophysical Research*, *115*(F3), F03008. https://doi.org/10.1029/2009JF001501

Plant, N. G., Holman, R. A., Freilich, M. H., & Birkemeier, W. A. (1999). A simple model for interannual sandbar behavior. *Journal of Geophysical Research: Oceans*, *104*(C7), 15755–15776. https://doi.org/10.1029/1999JC900112

Quartel, S. (2009). Temporal and spatial behaviour of rip channels in a multiple-barred coastal system. *Earth Surface Processes and Landforms*, *34*(2), 163–176. https://doi.org/10.1002/esp.1685

Radermacher, M., de Schipper, M. A., & Reniers, A. J. H. M. (2018). Sensitivity of rip current forecasts to errors in remotely-sensed bathymetry. *Coastal Engineering*, *135*, 66–76. https://doi.org/10.1016/j.coastaleng.2018.01.007

Ranasinghe, R., Symonds, G., Black, K., & Holman, R. (2004). Morphodynamics of intermediate beaches: A video imaging and numerical modelling study. *Coastal Engineering*, *51*(7), 629–655. https://doi.org/10.1016/j.coastaleng.2004.07.018

Rashid, A. H., Razzak, I., Tanveer, M., & Robles-Kelly, A. (2021). RipDet: A Fast and Lightweight Deep Neural Network for Rip Currents Detection. *2021 International Joint Conference on Neural Networks (IJCNN)*, 1–6. https://doi.org/10.1109/IJCNN52387.2021.9533849

Ruessink, B. G., Pape, L., & Turner, I. L. (2009). Daily to interannual cross-shore sandbar migration: Observations from a multiple sandbar system. *Continental Shelf Research*, *29*(14), 1663–1677. https://doi.org/10.1016/j.csr.2009.05.011

Ruessink, B. G., van Enckevort, I. M. J., Kingston, K. S., & Davidson, M. A. (2000). Analysis of observed two- and three-dimensional nearshore bar behaviour. *Marine Geology*, *169*(1–2), 161–183. https://doi.org/10.1016/S0025-3227(00)00060-8

Silva, A. D., Zhao, M., Stewart, D., Hasan, F., Dusek, G., Davis, J., & Pang, A. (2023). RipViz: Finding Rip Currents by Learning Pathline Behavior. *IEEE Transactions on Visualization and Computer Graphics*, 1–13. https://doi.org/10.1109/TVCG.2023.3243834

Simarro, G., Bryan, K. R., Guedes, R. M. C., Sancho, A., Guillen, J., & Coco, G. (2015). On the use of variance images for runup and shoreline detection. *Coastal Engineering*, *99*, 136–147. https://doi.org/10.1016/j.coastaleng.2015.03.002

Simarro, G., Calvete, D., Luque, P., Orfila, A., & Ribas, F. (2019). UBathy: A New Approach for Bathymetric Inversion from Video Imagery. *Remote Sensing*, *11*(23), 2722. https://doi.org/10.3390/rs11232722

Splinter, K. D., Holman, R. A., & Plant, N. G. (2011). A behavior-oriented dynamic model for sandbar migration and 2DH evolution. *Journal of Geophysical Research*, *116*(C1), C01020. https://doi.org/10.1029/2010JC006382

Thuan, D. H., Almar, R., Marchesiello, P., & Viet, N. T. (2019). Video Sensing of Nearshore Bathymetry Evolution with Error Estimate. *Journal of Marine Science and Engineering*, *7*(7), 233. https://doi.org/10.3390/jmse7070233

Ursell, F. "Short surface waves due to an oscillating immersed body." Proceedings of the Royal Society of London. Series A. Mathematical and Physical Sciences 220.1140 (1953): 90-103.

van Enckevort, I. M. J., & Ruessink, B. G. (2001). Effect of hydrodynamics and bathymetry on video estimates of nearshore sandbar position. *Journal of Geophysical Research: Oceans*, *106*(C8), 16969–16979. https://doi.org/10.1029/1999JC000167

Wright, L. D., & Short, A. D. (1984). *Morphodynamic variability of surf zones and beaches: a synthesis*. 26.